An optimized estimate of glacial melt from the Ross Ice Shelf using noble gases, stable isotopes, and CFC transient tracers

B. Loose,[1,2] P. Schlosser,[1,2,3] W. M. Smethie,[1] and S. Jacobs[1]

Received 26 July 2008; revised 28 February 2009; accepted 22 May 2009; published 12 August 2009.

[1] Isotopes of helium and neon and the $H_2^{18}O/H_2^{16}O$ ratio of water are proven proxies for melt from glacial ice beneath floating ice shelves and at ice shelf fronts. Their high concentrations in glacial meltwater, compared to other environmental sources, make them ideal tracers for studies of the pathways of glacial meltwater from its origins into the ocean interior. We combine noble gas and stable isotopes with temperature, salinity, and dissolved oxygen measurements from three cruises (along the Ross Ice Shelf during the austral summers of 1993–1994 and 1999–2000 and to the Ross Sea in 2000–2001) and use optimal multiparameter analysis to compute the water mass concentration, including glacial meltwater. The distribution of meltwater at the front of the Ross Ice Shelf extended east from 180°W, with the highest concentrations found near 165°W in both 1994 and 2000. The mean meltwater concentration at the ice shelf front was 2.0 ± 0.33‰ in 1994, 2.2 ± 0.36‰ in 2000, and 0.25 ± 0.1‰ in the western Ross Sea in 2001. Water mass concentrations are used to correct for bias in the CFC age, introduced by mixing with CFC-free waters, an effect revealed by comparing CFC age with transit time distribution curves. The water residence time within the ice shelf cavity, using CFCs and the mean meltwater concentration, implies a basal melt rate of 33–50 $km^3\ a^{-1}$.

Citation: Loose, B., P. Schlosser, W. M. Smethie, and S. Jacobs (2009), An optimized estimate of glacial melt from the Ross Ice Shelf using noble gases, stable isotopes, and CFC transient tracers, *J. Geophys. Res.*, *114*, C08007, doi:10.1029/2008JC005048.

1. Introduction

[2] Basal melting of ice shelves is an important component in ice sheet mass balance, both as a sink of glacial mass and as a process that can affect the stability of the ice shelf and the continental ice streams [*Alley et al.*, 2005]. Oceanographers and glaciologists have used a variety of techniques to estimate basal melt rates including heat and salt balances, box and stream tube models, [*Jacobs et al.*, 1985; *Smethie and Jacobs*, 2005], satellite-radar interferometry [*Rignot and Jacobs*, 2002] and numerical models [*Assmann et al.*, 2003; *Holland et al.*, 2003; *Rodehacke et al.*, 2006; *Dinniman et al.*, 2007]. A hydrographic time series from the Ross Sea indicates a freshening trend in recent decades that may result in part from meltwater production [*Jacobs et al.*, 2002]. According to modeling studies the basal melt rate should also be affected by interannual variability. For example, *Dinniman et al.* [2007] use a circulation model of the Ross Sea, including the ice shelf cavity, to demonstrate that the basal melt rate responds to external forcing (in this case an iceberg) within the time scale of 1 year. The model used by *Rodehacke et al.* [2006] to simulate melt beneath the Filchner-Ronne Ice Shelf (FRIS) produced an interannual variability of 24 $km^3\ a^{-1}$. This is 20% of the mean melt rate, but only 55% of the difference between previous data-based estimates of meltwater production (126 and 83 $km^3\ a^{-1}$, respectively [*Schlosser et al.*, 1990; *Joughin and Padman*, 2003]), which would indicate that "time-averaged" estimates still have room for improvement, before having to confront the effects of seasonal and other variability.

[3] The impetus to use tracers other than temperature and salinity for studies of basal melt arises from the need to separate the meltwater signal from other sources and sinks that modify these "conservative" properties. Each tracer is subject to potential biases, but the individual tracers represent an independent analog for the process of basal melting. Helium and neon are present in glacial ice as gas, trapped in air bubbles, or as clathrates (solute molecule surrounded by six water molecules) [*Namiot and Bukhgalter*, 1965]. When melting occurs at the base of the ice shelf, these gases are released and dissolve in the water. The low solubility of helium and neon in seawater ($\alpha \sim 0.008$ to 0.01) results in concentrations well above solubility equilibrium with the atmosphere (the primary source of helium and neon in the ocean), producing a glacial melt signal which can be traced from an ice front, across the continental shelf and into the abyssal ocean. *Schlosser* [1986] first demonstrated the utility of Δ^4He for studies of glacial meltwater production under-

[1]Lamont-Doherty Earth Observatory, Earth Institute at Columbia University, Palisades, New York, USA.
[2]Also at Department of Earth and Environmental Science, Columbia University, New York, New York, USA.
[3]Also at Department of Earth and Environmental Engineering, Columbia University, New York, New York, USA.

0148-0227/09/2008JC005048

neath ice shelves by comparing the helium isotope results to melt estimates derived from $\delta^{18}O$ along the FRIS. Subsequently, excess helium was used to estimate bottom water formation [*Weppernig et al.*, 1996] and glacial meltwater production rates of 0.004 Sv (126 km^3 a^{-1}) in the Weddell Sea [*Schlosser et al.*, 1990]. Helium and neon were used to derive estimates of meltwater production in the Pacific sector of the Southern Ocean, including the Amundsen and Bellingshausen Seas of 200–215 Gt a^{-1} (1 Gt $\sim$ 1 km^3 [*Hohmann et al.*, 2002], as compared to a previous estimate of 296 Gt a^{-1} [*Jacobs et al.*, 1996].

[4] While there are estimates of total ablation and mass balance for the major Antarctic ice shelves [*Rignot and Thomas*, 2002], most of the uncertainty in the estimates is associated with just two terms: calving and basal melt, which ranges from 25 to 100%. The challenge has been to refine and constrain the estimates of basal melt in an attempt to separate the trend from the natural variability [*Jacobs et al.*, 1996]. Here, we present an application of the optimal multiparameter (or multitracer) mixing analysis [*Tomczak and Large*, 1989] as a framework to combine the individual tracers and estimate the glacial meltwater concentration and distribution by treating glacial ice as one of the end-members, or source water types. We utilize potential temperature (θ), salinity (S), dissolved oxygen (O_2), ^{4}He, Ne, and $\delta^{18}O$ from three cruises to the Ross Sea, conducted in February 1994, February 2000 and February 2001. The OMP formalism has the advantage of representing a water parcel as a mixture of unique water types, or idealized values of each tracer representing the pure water mass, such that the fraction of each water type is mapped to the observational field, and intermediate concentrations represent the linear dilution of these water types. The estimation of glacial melt from a single tracer necessitates that the background or baseline concentration be established in order to separate the effect attributed to glacial melt. However, background concentrations are frequently difficult to assess because they represent the mixing between other water masses. In the OMP approach the baseline estimate can be avoided by treating each observation as a unique mixture of water types with well-defined tracer concentrations, whose spatial distribution can be ascertained from the mixture.

[5] In sections 2–5, we describe the hydrography of the Ross Sea and the observed tracer fields, briefly outline the architecture of the OMP method, and identify the sources from which the water-type matrix is estimated (section 2). In section 3, the distribution of water masses is reported and compared with the tracer distribution at the ice shelf front and in the Ross Sea. In section 4, we estimate the error introduced by unquantified sources in the individual tracers (e.g., terrigenic helium or marine ice formation), and by changes in the water type properties, over time. We compare the magnitude and distribution of glacial meltwater (GMW) concentration at the ice shelf front in 1994 and 2000, and in the Ross Sea in 2001. The water mass concentrations are used to correct the CFC concentration for the effects of dilution by water masses with no apparent CFC age, and subsequently used to recalculate the mean residence time inside the ice shelf cavity and the meltwater export. Finally, section 5 summarizes the advantages of a consistent and sufficient suite of water mass tracers as a means to monitor meltwater concentration and changes in circulation, as indicated by the spatial distribution of water masses.

2. Methods

2.1. Sample Collection and Measurement

[6] The sections along the Ross Ice Shelf (RIS) were completed in 1994 aboard the USCG icebreaker *Polar Sea* (PS94, 4–10 February 1994), and in 2000 aboard the *Nathaniel B. Palmer* (NBP00-01, 15 February through 21 March 2000). A total of 82 samples from NBP00-01 and 124 samples during PS94 contained simultaneous measurements of the stable isotope of water and noble gas tracers that are used in this study. From 15 February to 11 March 2001, the R/V *Italica* occupied a cruise track extending from west of Cape Adare (164°E) to the central Ross Sea near the continental shelf break (177°W) (Figure 1). In total, 191 data points were used from the 2001 cruise.

[7] He isotope and Ne samples were collected in copper tubes sealed by pinch-off clamps on both ends. The sample volume was approximately 40 ml. He and Ne samples were analyzed in the Lamont-Doherty Earth Observatory (LDEO) noble gas laboratory using a dedicated VG5400 mass spectrometer [*Ludin et al.*, 1998]. He, Ne and O_2 are reported in units of cm^3 STP g^{-1} and in the delta notation (e.g., $\Delta^4He = (^4He_{obs}/^4He_{eq} - 1) \times 100$), i.e., the percent deviation from solubility equilibrium with the atmosphere. For the mixing calculations, we use the absolute gas concentrations to avoid the complicating nonlinearities and possible errors in the solubility equations [*Top et al.*, 1987; *Hamme and Emerson*, 2004]. Precision of the ^{4}He and Ne concentrations is ±1% of the measured value.

[8] Samples for determination of $\delta^{18}O$ of water were collected in 100 ml glass bottles with a conical polypropylene cap. $H_2^{18}O/H_2^{16}O$ ratio measurements were performed at LDEO on a FISONS PRISM III Mass Spectrometer equipped with a MicroMass Multiprep automatic sample processing system after water sample equilibration with CO_2 using standard methods [*Epstein and Mayeda*, 1953; *Fairbanks*, 1982]. All samples were run in duplicate. Precision was estimated to be ±0.03 per mil (1σ) as determined by multiple daily analyses of laboratory standard DDW-2. Instrument linearity and accuracy was determined by comparison of DDW-2 to NBS standard water VSMOW, GISP, and SLAP. The accuracy is estimated to be within 0.03‰, or ±2% of the data range present in this paper, by comparison of measurements of North Atlantic Bottom Water with VSMOW. $\delta^{18}O$ samples are available from PS-94 and NBP00-01, but not for the 2001 *Italica* cruise. The O_2 samples used in this study are from bottle oxygen measurement using the titration standards of the World Ocean Circulation Experiment (WOCE) Hydrographic Programme Office [*Culberson and Williams*, 1991]. Duplicate samples taken throughout the cruise exhibited a mean difference of 0.006 cm^3 STP g^{-1} in 1994 and 0.038 cm^3 STP g^{-1} in 2000, which is less than 2% of the O_2 concentration range for samples used in this study.

[9] CFC-11, CFC-12 and CFC-113 were collected and measured aboard the NBP00-01 cruise, along the front of the Ross Ice Shelf, and aboard the *Polar Sea* in 1994. These data were used in a study to examine the evolution of CFC

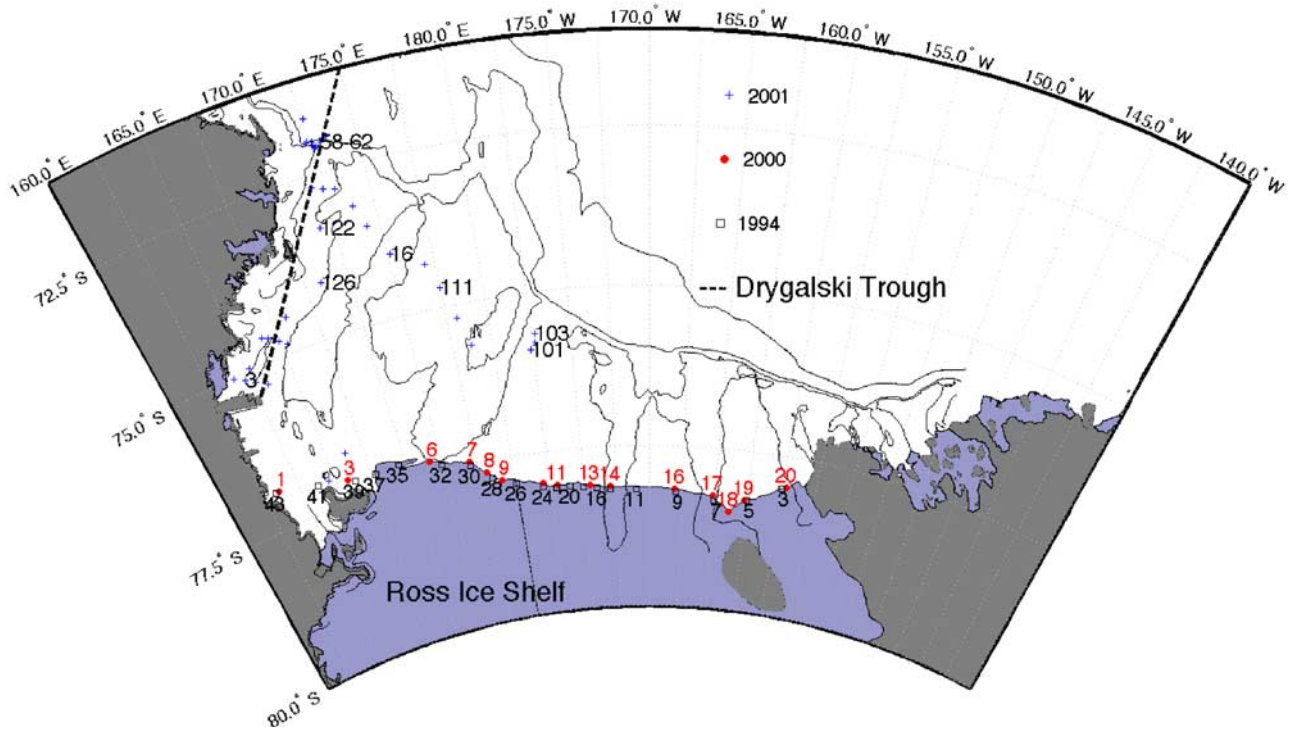

Figure 1. Stations along the Ross Ice Shelf and in the western Ross Sea from 1994, 2000, and 2001.

concentrations during a 16-year period [*Smethie and Jacobs*, 2005]. Here we use the same CFC data to infer the mean residence time of water beneath the Ross Ice Shelf.

2.2. Hydrographic Background

[10] As the Antarctic Circumpolar Current (ACC) enters the South Pacific, it takes a northerly excursion, guided by the Pacific-Antarctic Ridge, before returning southward offshore of the Amundsen and Bellingshausen Seas. Circumpolar Deep Water (CDW; $0.5 \leq \theta \leq 1.5$°C, S $\sim$ 34.7 psu) in the Pacific sector of the ACC is separated from shelf and surface waters at the Antarctic Slope Front [*Budillon et al.*, 2006]. Strong tidal mixing across the Antarctic Slope Front [*Padman et al.*, 2003; *Gordon et al.*, 2004] acts to produce a mixture of Antarctic Surface Water (AASW; $-1.6 \leq \theta \leq 1.0$°C, S < 34.2 psu) and Circumpolar Deep Water, that flows onto the continental shelf [*Smethie and Jacobs*, 2005] as modified CDW (mCDW: $\theta = -1.4$°C, S = 34.5). This water is thought to interact with the ice shelf at intermediate depths [*Smethie and Jacobs*, 2005]. The polynyas in the Western Ross Sea are major sources of shelf water formation in the Southern Ocean, generating High Salinity Shelf Water (HSSW; $\theta \sim -1.89$°C, S $\sim$ 34.8 psu), during the winter [e.g., *Budillon et al.*, 2006]. A portion of HSSW circulates under the floating ice shelf where it interacts with the glacial ice, and emerges as a slightly freshened, plume near the dateline at about 500 m depth (stations 10–13 in 2000 (Figure 2) [*Smethie and Jacobs*, 2005]).

2.3. Multitracer Mixing Analysis

[11] The method of optimal multiparameter (multitracer) analysis (OMP) [*Tomczak and Large*, 1989] uses a nonnegative least squares approach to calculate the source water distributions as a fraction of the total water mixture at any sampling location, p. The problem can be formulated given n linearly independent conservative tracers, and m $\leq$ n unique water types:

$$\text{minimize } \| \mathrm{Cf} - \mathrm{y} \|^2, \text{ subject to } \mathrm{f} \geq 0 \qquad (1)$$

where **C** is the matrix of source water types, **y** is the vector of measured concentrations at sampling location, p, and f is the fraction of each water type present at p. Physically, the water mass fractions, f_i must only vary between 0 and 1 to preserve continuity. This constraint necessitates an iterative solution, and must satisfy the Kuhn-Tucker theorem [*Menke*, 1989]. An algorithm for solving equation (1) using the Kuhn-Tucker condition is described by *Menke* [1989] and *Lawson and Hanson* [1974]. Similar optimization methods are presented by *Press et al.* [1992]. *Tomczak and Large* [1989] provide more detail on the application of a nonnegative least squares approach to water mass mixing. Because the OMP method reproduces the observed tracer fields by mixing only, it has difficulty with sample points near the sea surface where ocean-atmosphere exchange affects the water mass tracers to a magnitude that is not explicitly accounted for [*Tomczak and Large*, 1989]. In this study, samples above 100 m depth are excluded from the estimate of the mean and maximum glacial meltwater concentration.

[12] For the mixing analysis, we consider the four primary water masses in the Ross Sea to be AASW, HSSW, CDW, and glacial ice, which is transformed into glacial meltwater (GMW). In a similar study, *Budillon et al.* [2003] used a different set of source water type definitions, including Low Salinity Shelf Water (LSSW) and modified CDW (mCDW), to describe the Ross Sea on the basis of the hydrography outlined by *Jacobs et al.* [1985]. However, it can be difficult

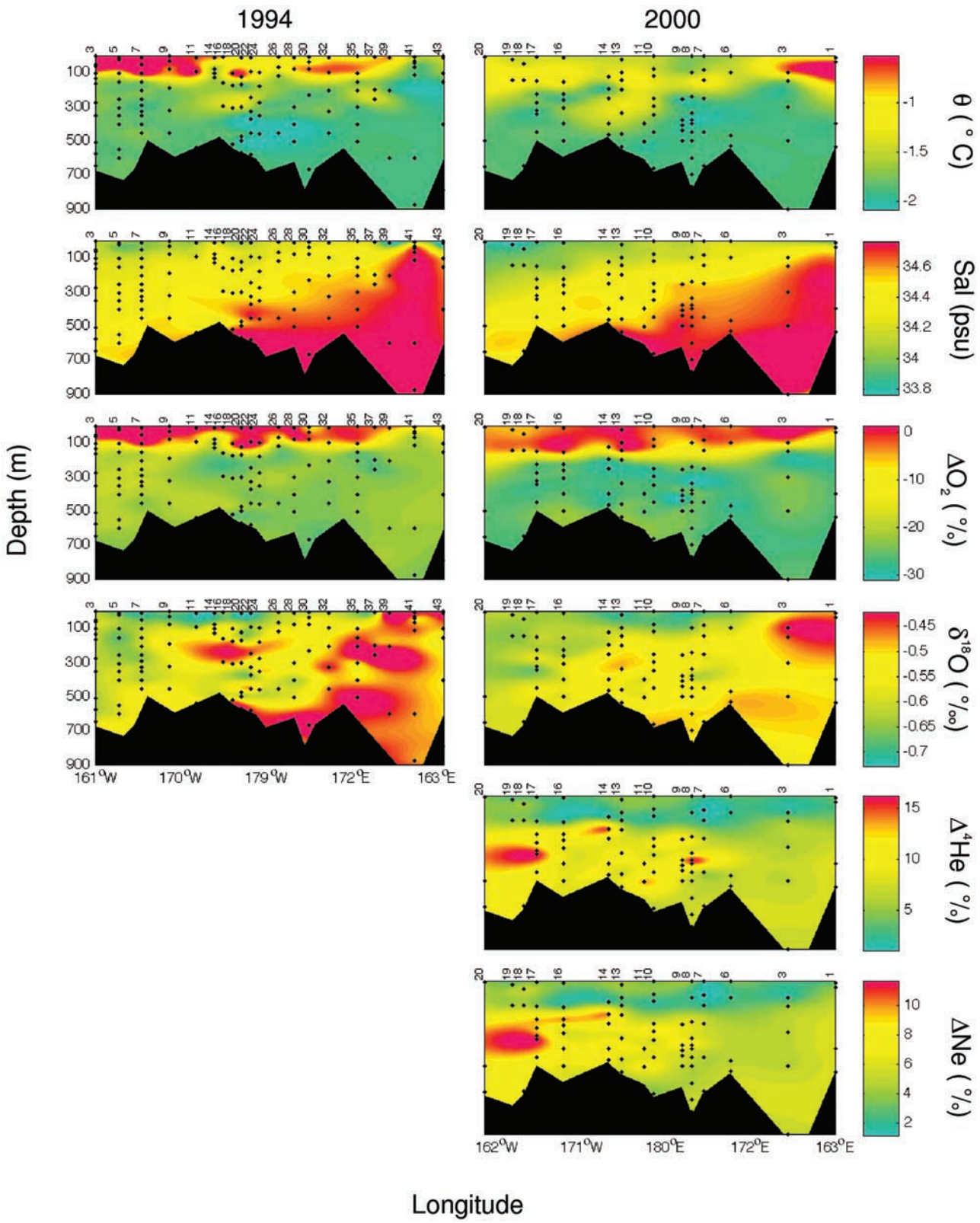

Figure 2. Sections of water mass tracers θ, S, O_2, and $\delta^{18}O$ (1994 and 2000) as well as Δ^4He and ΔNe in 2000 along the front of the Ross Ice Shelf. Each plot is oriented looking south, with the eastern Ross Sea on the left.

Table 1. Characteristic Values for the Water Mass Tracers θ, S, ^{4}He, Ne, δ^{18}O, and O_2 in the Water Type Matrix C[a]

	AASW (1994/2000–2001)	HSSW (1994/2000–2001)	CDW	Glacial Ice
θ (°C)	−0.9/−1.2	−1.89/−1.88	1.17	$-2.6 - (\rho_{ice}L_f)/(\rho_{water}C_p)$
S (psu)	34.05/34.1	34.81/34.75	34.70	0.00
δ^{18}O (‰)	−0.62/−0.63 ± 0.03	−0.44/−0.50 ± 0.03	−0.07 ± 0.03	−40.90 ± 1.5
[Ne] × 10^{-8} cm^3 STP g^{-1}	Not used/18.56 ± 0.2	Not used/18.8 ± 0.2	Not used/17.7 ± 0.2	Not used/200 ± 6.5
[^{4}He] × 10^{-8} cm^3 STP g^{-1}	Not used/4.13 ± 0.04	Not used/4.28 ± 0.05	Not used/4.19 ± 0.04	Not used/57.60 ± 1.9
[O_2] × 10^{-3} cm^3 STP g^{-1}	8.05/8.08 ± 0.04	6.28/6.19 ± 0.04	4.18 ± 0.03	19.51 ± 1.9

[a]The values for AASW and HSSW change with time; we have defined one set of values for 1994 and another set of values for 2000 and 2001.

to establish characteristic values for these intermediate water types. In contrast, pure CDW and glacial meltwater are source water types whose properties are not as time-variant, and we find that the mixture of CDW and AASW is effective at describing the intermediate mixtures of mCDW and LSSW.

2.4. End-Member Properties

[13] The characteristic values of each tracer in the four source water types under consideration were defined to reflect the most general characteristics of those water masses. However, given the cooling and freshening tendency observed in the Ross Sea [*Jacobs et al.*, 2002], the locally formed water masses, HSSW and AASW, were defined using data that coincides with the data under consideration. CDW and GMW in their pure form can be defined from preexisting data. The characteristic values of each water type are listed in Table 1. HSSW and AASW have unique values in 1994 and 2000–2001. The salinity and potential temperature of AASW is taken as the average within 50 m of the surface (1994: 34.05 psu, −0.9°C; 2000–2001: 34.1 psu, −1.2°C). The δ^{18}O of AASW during both years is the same, within analytical precision (1994: −0.62 ± 0.03‰; 2000: −0.63 ± 0.03‰). HSSW was assumed to be the most saline water mass (1994: 34.81 psu; 2000–2001: 34.75 psu); temperature and δ^{18}O were defined from the average of the most saline samples (1994: −1.89°C, −0.44 ± 0.03‰; 2000–2001: −1.88°C, −0.50 ± 0.03‰). The salinity, temperature and δ^{18}O in CDW are 34.7 psu, 1.17°C and −0.07‰, respectively [*Jacobs et al.*, 1985]. The salinity of glacial meltwater is assumed to be zero, and the temperature is derived from heat conservation. The temperature upon melting can be estimated as the depth-dependent freezing point temperature, less the latent heat of fusion, $T_m = T_{fp} - \Delta T_{Lf}$, where T_m is a function of salinity and pressure [*Holland and Jenkins*, 1999]. $\Delta T_{Lf} = \rho_{ice}L_f/\rho_{fw}C_p$ where L_f and C_p are the latent heat of fusion and the specific heat capacity of water. ρ_{ice} and ρ_{sw} are the densities of ice and freshwater. They are treated as constants in this calculation, and their variability has little effect on the magnitude of ΔT_{Lf}.

[14] The concentration of ^{4}He, Ne and O_2 in AASW were similarly defined from data at the ice shelf front. For AASW the average surface layer value was O_2 = 8.05 ± 0.04 × 10^{-3} cm^3 STP g^{-1} in 1994. In 2000, the gas concentration in AASW was Ne = 18.56 ± 0.2 × 10^{-8}, ^{4}He = 4.13 ± 0.04 × 10^{-8} and O_2 = 8.08 ± 0.04 × 10^{-3} cm^3 STP g^{-1}. The gas concentration in HSSW was estimated in the same manner as θ and δ^{18}O: O_2 = 6.28 ± 0.04 × 10^{-3} cm^3 STP g^{-1} in 1994. In 2000, Ne = 18.8 ± 0.2 × 10^{-8}, ^{4}He = 4.28 ± 0.05 × 10^{-8} and O_2 = 6.19 ± 0.04 × 10^{-3} cm^3 STP g^{-1} in HSSW. O_2 in CDW was estimated by matching the temperature maximum from 2001 with the T-S properties at stations near Cape Adare, during the WOCE Hydrographic Program S04P cruise in 1992. *Hohmann et al.* [2002] estimated the concentration of ^{4}He, Ne, and O_2 in glacial ice as 57.6 ± 0.19 × 10^{-8} cm^3 STP g^{-1}, 200.0 ± 6.5 × 10^{-8} cm^3 STP g^{-1}, and 19.51 ± 1.9 × 10^{-3} cm^3 STP g^{-1}, respectively. To avoid the nonlinear dependence of Δ^4He, ΔNe and ΔO_2 on θ and S [*Hohmann et al.*, 2002] the mixing analysis was performed using the absolute noble gas concentrations instead of the Δ notation. The dependence on water density, if neglected, introduces an error of approximately 1.3% over the range of density in the data sets under examination. This effect is smaller than the nonlinearity associated with solubility. The estimate of δ^{18}O in glacial ice was taken from the National Snow and Ice Data Center ice core stacks [*Grootes et al.*, 1995]. The two cores closest to our sample region were Taylor Dome and Dominion Range, with average δ^{18}O values of −39.9 ± 1.5‰ and −41.9 ± 1.6‰, respectively. We used a value of −40.9‰.

3. Results

3.1. Ross Ice Shelf

[15] δ^{18}O in both 1994 and 2000 has the highest values (∼−0.42‰) in the western part of the section (Figure 2: station 37 in 1994 and station 3 in 2000), where the Ross polynya is typically situated in winter. δ^{18}O also highlights the core of CDW that coincides with a subsurface maximum in temperature between 200 and 500 m, near 175°W. The lightest values (δ^{18}O ∼ −0.7‰) coincide with the maximum Ne excess. The distribution of neon along the front of the Ross Ice Shelf negatively covaries with potential temperature (Pearson's r = −0.57 (Figure 3)). Both Ne and θ depict two cores of Ice Shelf Water in 2000; the first corresponds with a tongue of water, between 300 and 600 m, as cold as θ = −2.1°C, between stations 8 and 11 (Figure 2). The second core to the east, between stations 14 and 16 at 200–300 m depth, exhibits the highest values of Δ^4He = 16.2% and ΔNe = 11.7% in 2000, with $\theta < -1.8$°C. The ΔO_2 at the ice shelf front is closest to saturation above 100 m. Below 100 m, the features are subtle, but ΔO_2 is greatest in the east at stations 3, 5 and 7 in 1994 and at station 20 in 2000.

[16] The CFC data collected at the ice shelf front exhibit undersaturation with respect to the solubility equilibrium with the atmosphere throughout the majority of the section. The highest concentrations exist in the Western Ross Sea, near Ross Island. This region is known for the presence a persistent polynya, exposing the mixed layer to the atmosphere for the majority of the year. The HSSW that is formed in this region is marked by a CFC signal reaching to depths of up to 900 m in the Western Ross Sea [*Smethie and Jacobs*, 2005]. Because of the connection between the deep CFC

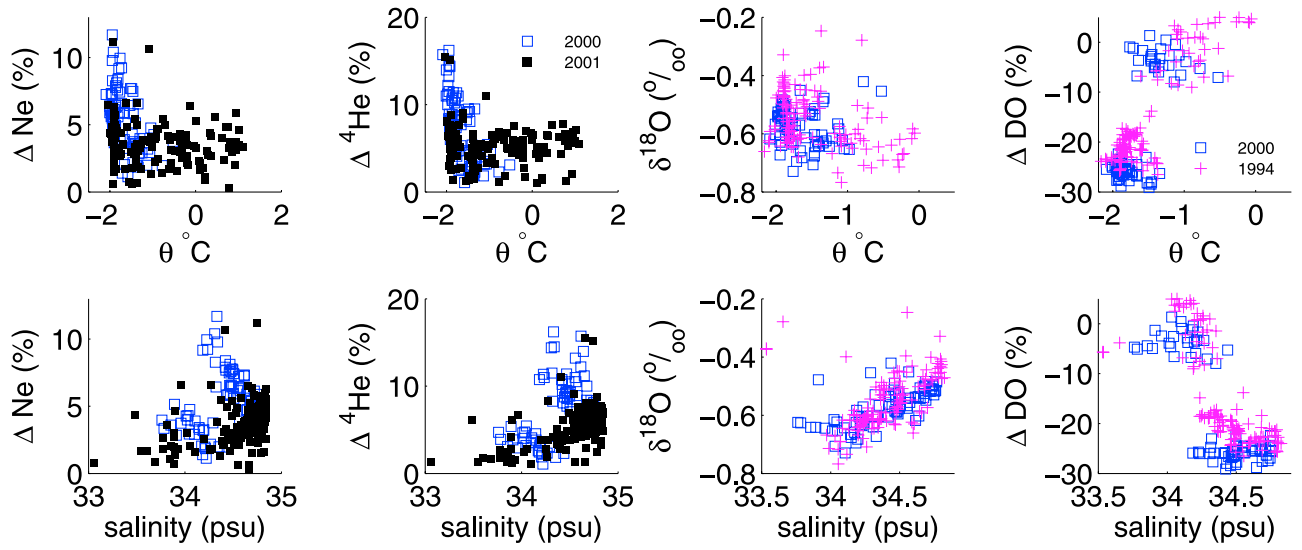

Figure 3. Property diagrams of θ and S versus ΔNe, Δ^4He, δ^{18}O, and O_2 from the front of the RIS in 1994 and 2000 and in the Ross Sea in 2001. ΔNe and Δ^4He were not collected on the *Polar Sea* in 1994; δ^{18}O and O_2 were not available from the 2001 cruise.

signal and the Ross Sea polynya, we use the surface values in the western Ross Sea to correct for undersaturation. The saturation levels of CFC-11, CFC-12, and CFC-113 were 89%, 94%, and 81%, respectively, in 2000. The 1994 saturation levels of CFC-11, CFC-12, and CFC-113 were estimated to be 91%, 97%, and 88%, respectively. The order of increasing saturation between the gases is consistent with the order of the diffusion coefficients [*Wanninkhof*, 1992; *Zheng et al.*, 1998; *Postlethwaite et al.*, 2005]. CFC data are presented in terms of their equivalent partial gas pressure (pCFC), which represents concentration, normalized by temperature and salinity-dependent solubility.

3.2. Ross Sea

[17] The 2001 stations are concentrated in the western Ross Sea, along the Drygalski trough, and along a NW–SE section landward of the continental shelf break (Figure 1). A series of 8 stations located near the northern extent of the trough, extend to the 1900 m isobath, where the Antarctic Slope Front moves on and off the shelf with the tides [*Whitworth and Orsi*, 2006]. There are few traces of high excess helium along the Drygalski Trough (Figure 4); a single broad peak in Δ^4He and ΔNe reaches a maximum near 400 m. The helium and neon signals are strongest to the east of 180°W (station 101). The maximum values of Δ^4He (15.5%) and ΔNe (11.2%) are found at stations 102 and 103 (adjacent to station 101 (Figure 1)), furthest to the east, and coincide with potential temperatures below −2°C (Figure 3). The correlation between θ and ΔNe is r = −0.27 in 2001, and indicates a different tendency than at the ice shelf front, especially between deep stations away from the shelf. The minimum excesses at the surface are characterized by Δ^4He and ΔNe values of ∼1% and they coincide with a salinity minimum. Supersaturated He and Ne at the surface may be an indication of meltwater presence, whose gas concentration has been preserved by the presence of partial ice cover. Alternately, sporadic sea ice formation or bubble mediated gas exchange by breaking waves could also produce gas excesses near the air-sea interface.

3.3. Water Mass Fractions

[18] The OMP-derived water mass fractions were calculated using θ, S, O_2, ^{4}He, Ne and δ^{18}O from the 2000 data set, whereas ^{4}He and Ne were not sampled with sufficient frequency to be included in the 1994 estimate. In Figure 5, the white contour lines indicate the mean water mass concentration. In 1994, HSSW occupied much of the western portion of the ice shelf front, with mass fractions greater than 0.9 extending as far up in the water column as 100 m in the region of the Ross Sea polynya, then deepening east of 172 °E in 1994 and 2000 (Figure 5). AASW was most concentrated just below 100 m depth (f = 0.89) at station 20, in 1994, but penetrated to the bottom at stations 3 (f = 0.12 at 650 m) and 11 in the Eastern Ross Sea. In 2000, AASW was confined above 300 m. The mean salinity between 100 and 200 m was 0.14 psu fresher in 2000 as compared to 1994,

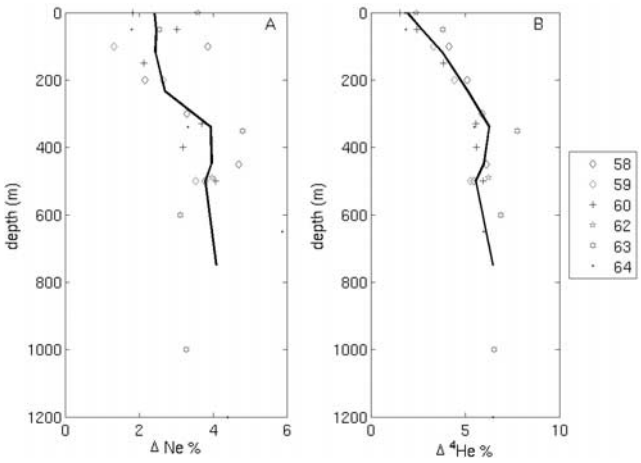

Figure 4. ΔNe and Δ^4He from six stations near the offshore outlet of the Drygalski trough. Stations are located within a 30 km radius of each other. The black line indicates a three data point vertical moving average of the stations.

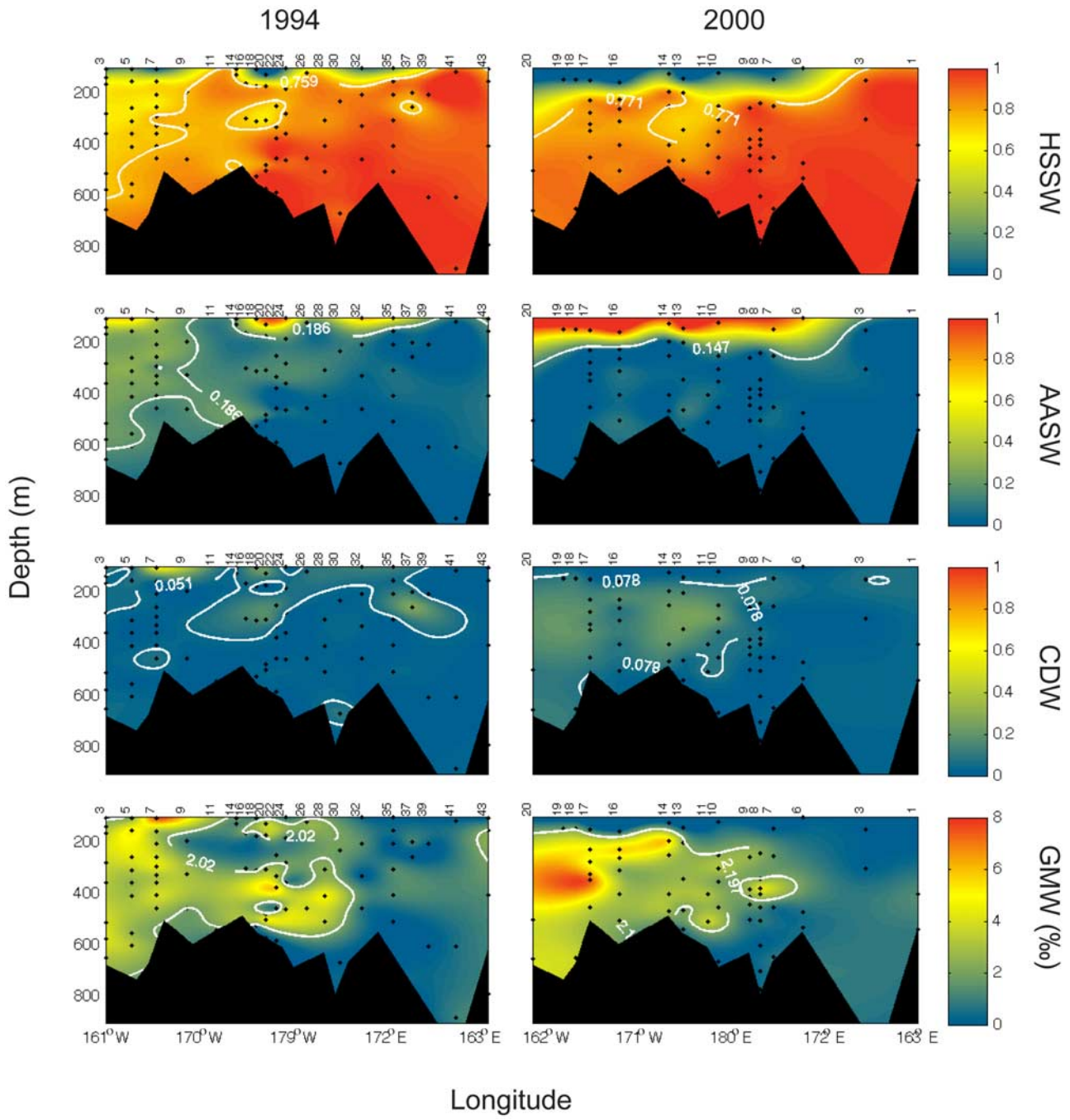

Figure 5. Water mass fractions derived from the OMP method using θ, S, $\delta^{18}O$, and O_2 in 1994 and θ, S, $\delta^{18}O$, O_2, Ne, and ^4He in 2000. The orientation is toward the south, with the eastern Ross Sea on the left side of each plot.

favoring greater concentration of AASW. In 1994, the mean value of AASW (0.186) penetrated below 400 m between 160 and 173°W, in contrast with 2000. In this region, O_2 is 7% more saturated in 1994 and O_2 saturation in 1994 and $\delta^{18}O$ is 0.04‰ lower, on average, which would produce a greater quantity of AASW.

[19] The spatial distribution of CDW extends from 200 to 600 m, east of 175°E in 1994 and in 2000. In 2000, CDW was most distinct at station 13 near 300 m depth (f = 0.23). A similar feature is evident in the 1994 section at station 16 (300 m depth, Figure 5), however the distribution of CDW was shifted vertically in 1994, with concentrations above the mean (f = 5.1% at 100 m along much of the ice shelf front (east of 165 °E), corresponding with low values in $\delta^{18}O$.

4. Discussion

4.1. Glacial Meltwater at the Ice Shelf Front and in the Ross Sea

[20] The samples collected at the front of the Ross Ice Shelf provide estimates of the GMW distribution in the same region separated by a 6-year period, from 1994 to 2000.

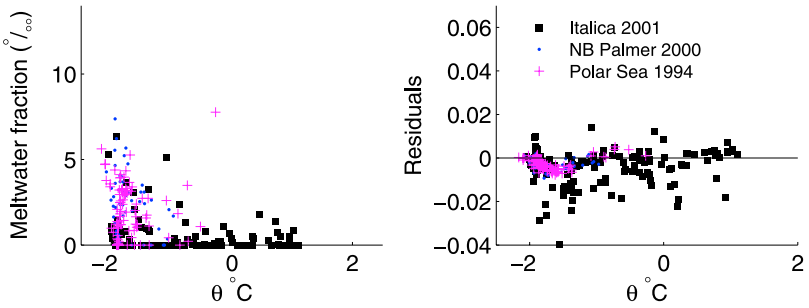

Figure 6. Glacial meltwater fractions and the residuals, or sum of water mass fractions minus one, plotted as a function of temperature from the 1994, 2000, and 2001 cruises. The OMP-derived sum of the water mass fractions is an indication of the fit quality: water mass fractions should sum to one.

However, before comparing these estimates, it is important to consider the sources of variability that exist in the OMP-derived GMW calculation. In this section we describe the distribution of GMW at the ice shelf front. Irregular sample distribution can affect the resulting water mass estimates, placing preferential emphasis on isolated samples. Using a bootstrap analysis we have determined the sensitivity of the solution to the existing collection of samples. The residuals from the OMP solution were randomly sampled, with 1500 iterations, to reconstruct the water mass fractions [*Mooney and Duval*, 1993]. This produces a nonparametric distribution of the mean and maximum GMW fractions, which are presented at the 95% confidence. In section 4.2, we attempt to constrain the other sources of variability: the bias introduced by using a different suite of tracers in 1994 as compared to 2000 and the effect of changing water type properties on the water type matrix, **C**.

[21] The quality of the fit between the four end-member optimal mixing model using HSSW, AASW, CDW and glacial ice can be viewed through the adherence to the continuity constraint; the water mass fractions at each sample point must sum to one. Figure 6 shows the GMW fractions plotted versus temperature and the residuals, or sum of the water mass fractions minus one, at each point for the three cruises. The anomalous high GMW fraction at −0.26°C is found near 100 m at station 7, reflecting the high concentration of O_2 and low $\delta^{18}O$ value in the mixed layer. The GMW fractions from 2001 stations span a much wider range in temperature; samples with temperatures above −0.5°C have low GMW contents (<2‰). The maximum magnitudes in the residuals for the 1994, 2000, and 2001 data are 0.017, 0.01, and 0.039, respectively. The residuals all lie within 5% of the expected value from the continuity constraint, which has been used as the acceptable limit for reporting water mass fractions [*Poole and Tomczak*, 1999; *Budillon et al.*, 2003]. The residuals are greatest in the 2001 data set, as it spans the greatest spatial extent including stations off the continental shelf, which may not be as well represented by the four water types that we have employed in this study.

[22] During both 1994 and 2000, most of the GMW was confined to the eastern half of the ice shelf front, while the largest concentration of HSSW was found on the western shelf (Figure 5). By resampling the residuals at 95% confidence, the mean GMW fraction along the RIS in 2000 was 2.2 ± 0.1‰, with a maximum fraction of 7.3 ± 0.7‰. In 2000, the highest GMW fraction is observed near 400 m depth, coinciding with the maximum Ne excess in Figure 2. This warmer and fresher water mass is attributed to the penetration of CDW in its modified form (mCDW: $\theta = -1.4$°C, S = 34.5 psu) below the ice shelf, whereas the deeper outflow near station 10 (Figure 2) correlates with the coldest temperatures ($\theta \leq -2.1$). The GMW fractions during 1994 followed the 2000 pattern, but the concentrations were smaller, with a mean value of 2.0 ± 0.1‰ and a maximum of 6.8 ± 1.1‰. In 1994 a greater portion of the GMW was concentrated in the surface layers of the Ross Sea, which coincided with the lowest $\delta^{18}O$ values in the section (−0.76‰), as well as dissolved oxygen close to saturation (∼95%). The low $\delta^{18}O$ values can result from precipitation (addition of isotopically light rain or snow), and the high value of oxygen may be produced by photosynthesis, sea ice formation or bubble-mediated gas exchange with the atmosphere. These processes exhibit a similar signature to the input of glacial meltwater, potentially producing a GMW artifact in the surface layer. The shallow maximum in GMW was not present in 2000, when Δ^4He and ΔNe values in the mixed layer were 3 times lower than in the ISW maximum (between 200 and 400 m). Whereas it is possible that the meltwater signal in the mixed layer is valid, but is not reflected in Δ^4He and ΔNe because of gas evasion to the atmosphere, it is difficult to deconvolve the multitude of processes that alter meltwater tracers in the surface layers. For this reason, the top 100 m of the water column are not considered in the GMW inventory and the estimate of basal melt rate.

[23] The mean and maximum fractions of GMW at the 2001 stations in the Ross Sea were 0.25 ± 0.3‰ and 5.7 ± 0.7‰ (Figure 7). The greatest GMW concentration, north of the ice shelf, was located north and west of the highest concentrations at the ice shelf front, along 2001 stations 101–103 (Figure 8), a short distance east of the dateline.

[24] To estimate the inventory of GMW in the Ross Sea, we multiplied the average GMW concentration by the volume hypsograph based on data by F. J. Davey and F. Nitsche (Bathymetric grid of the Ross Sea, Antarctica, 2005, ftp://ftp.ldeo.columbia.edu/pub/fnitsche/RossSeaBathymetry), not including the volume under the Ross Ice Shelf. In the hypsographic calculation, the 1500 m isobath was used as the ocean boundary for the Ross Sea. The total meltwater in the Ross Sea, derived from 2001 stations was ∼74 km^3. However, this estimate is based on a very uneven sample distribution with no data coverage east of 175°W.

[25] The distribution of GMW in the western Ross Sea deepens and broadens as compared with the distribution at the front of the Ross Ice Shelf. We calculated the first and

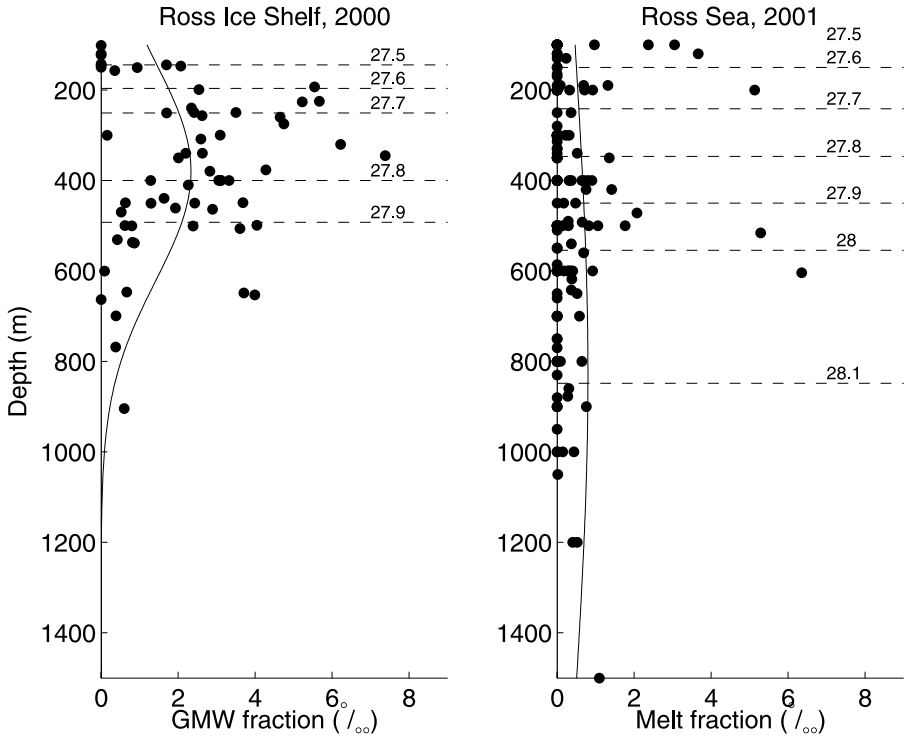

Figure 7. Depth profiles of glacial meltwater fraction (in ‰) (left) along the front of the RIS in 2000 and (right) in the central Ross Sea from 2001 data. The horizontal dashed lines indicated isopycnals in (σ_θ). The solid black line is a Gaussian fit to the data using the first and second moment of the concentration distribution, although the scatter in data is too high to produce a statistically significant fit to the data. The first moment of GMW fractions deepens from 365 m at the Ross Ice Shelf to 696 m in the Ross Sea at the 2001 stations.

second moment of the GMW distribution; the centroid of the plume at the RIS was 365 ± 200 m at a potential density anomaly close to $\sigma_\theta = 27.8$, which is very near the neutrally buoyant density for the deep core of Ice Shelf Water ($\theta < -2°C$, S = 34.5 psu, $\sigma_\theta = 27.78$). In the Ross Sea, the centroid of the plume has shifted downward to 696 ± 400 m, below a density of $\sigma_\theta = 28.0$ (Figure 7), although the scatter in the data is too large to produce a statistically significant fit. This

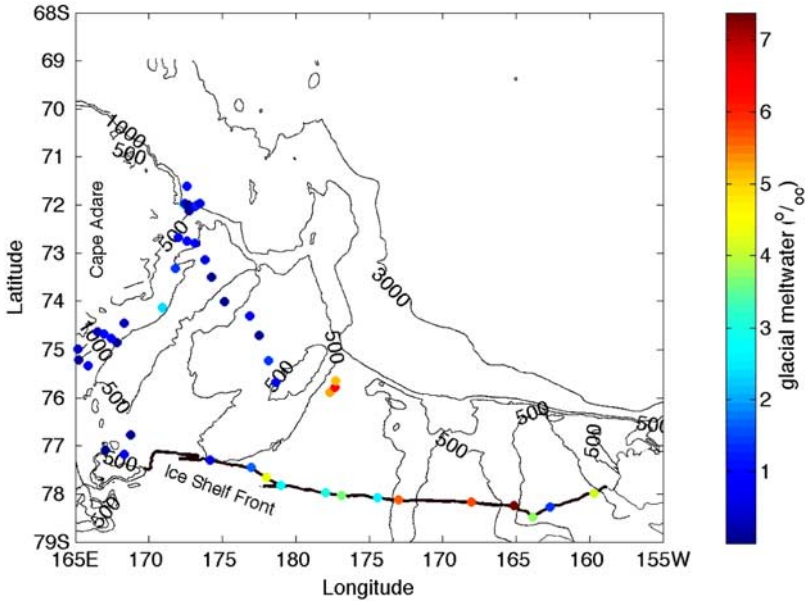

Figure 8. The maximum glacial meltwater content (in ‰) at the front of the Ross Ice Shelf, taken from the transect in 2000, and in the western Ross Sea in 2001.

Table 2. Mean ($\bar{f}$) and Maximum (f_{max}) Meltwater Fraction in 2000 Determined by Sequentially Excluding One Tracer and Computing the Mean and Maximum Fractions With the Remaining Tracers[a]

Excluded Tracer	$\bar{f}$ GMW (‰)	f_{max} GMW (‰)
None	2.2	7.3
θ (°C)	2.8	9.3
S (psu)	1.7	5.4
$\delta^{18}O$ (‰)	2.5	8.4
[Ne] $\times 10^{-8}$ cm^3 STP g^{-1}	2.0	6.7
[^{4}He] $\times 10^{-8}$ cm^3 STP g^{-1}	2.2	7.1
[O_2] $\times 10^{-3}$ cm^3 STP g^{-1}	2.2	7.4

[a]In 2000, the availability of six water mass tracers ensures that the OMP solution is still overdetermined, after the exclusion of one tracer.

deepening and broadening of the GMW curve could be the result of diapycnal mixing (gas exchange will eliminate the He and Ne signal in the surface waters, which would give the appearance of a deeper centroid). The western Ross Sea is known to be a region of high vertical shear and mixing. Alternately, the apparent deepening and broadening of the plume could instead be evidence of a remote source such as inflow of meltwater from the Amundsen Sea, to the east [*Hohmann et al.*, 2002; *Jacobs et al.*, 2002], but it is difficult to determine this influence, because of lack of samples near the shelf slope break east of 175°W.

4.2. Sources of Bias and Uncertainty in the Meltwater Concentration

[26] To achieve an overdetermined solution to the optimal water mass calculation requires at least as many water mass tracers as water masses. In this analysis we have used as many independent tracers as were available in each of the data sets. As a consequence, our estimates of GMW are not based on the same set of tracers during each cruise. Furthermore, several of the tracers are subject to unquantified modifications that can bias the estimate of GMW. For example, P. Schlosser et al. (manuscript in preparation, 2009) have noted an anomalously low ^{3}He/^{4}He ratio in the plume of glacial meltwater water found in the central Ross Sea near 500 m depth. They postulate that this water contains helium from a terrigenic source, i.e., a mixture of radiogenic helium (^{3}He/^{4}He $\approx 2 \times 10^{-8}$) and mantle helium (^{3}He/^{4}He $\approx 1 \times 10^{-5}$). This extra source complicates the glacial meltwater signal, as expressed through helium, and samples with a helium ratio below ^{3}He/^{4}He = 1.355×10^{-6} [*Clarke et al.*, 1976; *Benson and Krause*, 1980] may be affected by terrigenic helium. The potential for marine ice formation exists when Ice Shelf Water near the freezing temperature, rises buoyantly within an ice shelf cavity [*Bombosch and Jenkins*, 1995], as is the case below the RIS and the FRIS. *Schlosser et al.* [1990] suggest that marine ice formation preferentially rejects salt and only slightly decreases $\delta^{18}O$ in Ice Shelf Water as compared to dissolved He and Ne, which might be included as clathrates within the ice matrix. Finally, dissolved oxygen is subject to biological production and consumption.

[27] To gauge the possible bias introduced into the GMW estimate by using different water mass tracers with their respective artifacts, we used a resampling procedure, sequentially discarding one tracer (θ, S, ^{4}He, Ne, $\delta^{18}O$, O_2) and recalculating the GMW fractions. The resampling calculation was performed on the 2000 section along the ice shelf front, when all six water mass tracers were measured. The exclusion of temperature and salinity produce the greatest changes in the mean GMW fraction: $\bar{f}$ = 2.8‰ and 1.7‰, respectively, which is a maximum of 27% difference from the mean fraction when all tracers are used ($\bar{f}$ = 2.2‰). The exclusion of $\delta^{18}O$ and Ne caused a 13% increase and a 10% decrease in $\bar{f}$, respectively. The effect of excluding ^{4}He and O_2 was to decrease the mean GMW fraction by less than 1%. The values of $\bar{f}$ and f_{max} are summarized in Table 2. If both ^{4}He and Ne are not used in the OMP calculation, as in 1994, the mean GMW concentration decreases by 23% from 2.2 to 1.7‰, and $\bar{f}$ of CDW decreases by 32% from 0.078 to 0.053. These differences must be considered when comparing estimates of water mass fractions from the 1994 and 2000 survey, and this error is larger than the observed change in the mean water mass fraction of both CDW and GMW during this 6-year period (Figure 6).

[28] The successive exclusion of a water mass tracer and recalculation of the GMW fraction demonstrates the variability introduced by using a differing set of tracers and their associated biases. However, the water mass fractions are also affected by uncertainty in the characteristic values of the source water types, which are subject to change as shown by *Jacobs et al.* [2002]. We use the expectance for the ordinary least squares case to examine the change in variance of the water mass concentration, f, that is produced by changes in the water type matrix **C**, $\mathrm{Var}[f] = (\mathbf{C}^T\mathbf{w}^T\mathbf{w}\mathbf{C})^{-1}\mathbf{C}^T\mathbf{w}^T\mathbf{w}\boldsymbol{\Sigma}_y$, where **w** is a weight matrix reflecting the measurement precision of the tracers and $\boldsymbol{\Sigma}_y$ is the covariance matrix of **y**, i.e., the observations of (θ, S, ^{4}He, Ne, $\delta^{18}O$) at each point. When we separately propagate a perturbation in salinity and temperature in HSSW and AASW through the OMP calculation, the change in the Var[f] is ~8% per psu and 14% per degree Celsius. Using the same perturbations, a forward sensitivity analysis proved that the mean GMW fraction $\bar{f}$ changed by a similar magnitude as the variance in f. The observed trend in salinity and temperature [*Jacobs et al.*, 2002], would imply that values of AASW and HSSW in **C** change by ~1% of the range in temperature and salinity, per year. If the errors in temperature and salinity are additive, this would produce ~4% change in the GMW fraction, between 1994 and 2000.

[29] This exercise highlights one benefit of the OMP formalism; the calculation can be used to systematically probe the sensitivity of the solution to different sources of error that result from the inclusion of different tracers and from variability introduced by changes in the water type properties over time. It is apparent that the biases between water mass tracers and inconsistencies in the water type properties exceed the effect of analytical error for any of the six tracers included in this analysis. In summary, comparison of repeat surveys for GMW concentration in 1994 and 2000, are subject to ~23% uncertainty due to the use of a different suite of tracers, and ~5% uncertainty as a result of changing water mass properties over time.

4.3. CFC Age Distribution and Cavity Residence Time

[30] The new information derived from the water mass tracers provides an opportunity to reexamine the cavity residence time under the Ross Ice Shelf. Using the CFC data presented by *Smethie and Jacobs* [2005], we correct for sev-

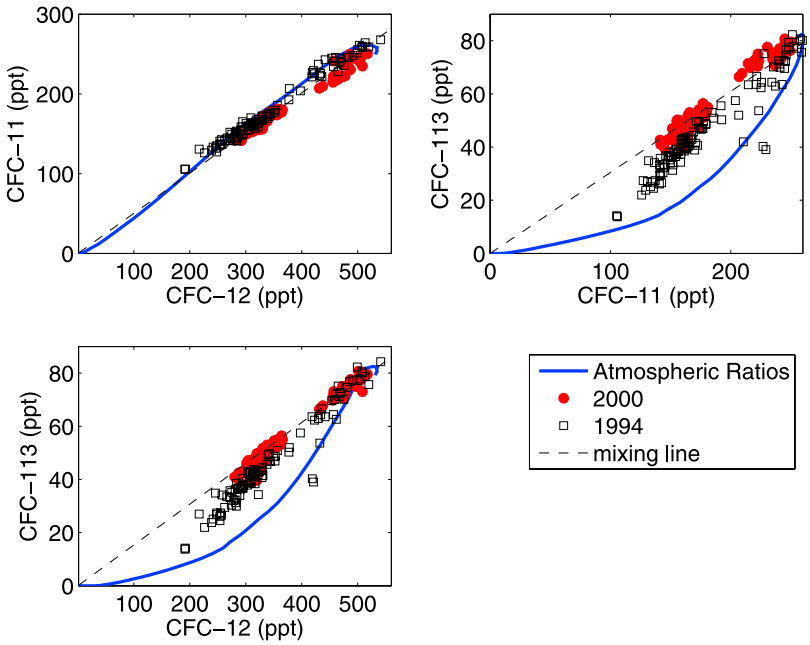

Figure 9. Plots of CFC partial pressure (pCFC): CFC-11 versus CFC-12, CFC-113 versus CFC-12, and CFC-113 versus CFC-11 from data collected at the RIS front in 2000 (red circles) and 1994 (black squares). The blue line indicates the CFC ratio from the atmospheric concentration history, and the dashed line is meant to indicate a mixing between water of zero-CFC concentration and modern ratios, reflecting the years of 1990–2000.

eral factors that may bias the relative CFC age of the different water masses.

[31] The ratio of CFC concentration at the ice shelf front does not display the full range of values indicated by the atmospheric time history of the CFCs [*Walker et al.*, 2000]. Instead, a remarkably constant ratio extends from modern concentrations toward zero, as indicated by the dashed line in Figure 9. This is indicative of a mixing line between zero concentration and modern CFC ages, which suggests that the seasonally ventilated waters of the continental shelf are mixing with "old" water masses that have little or no detectable CFC concentration, i.e., CDW and/or GMW. The constant slope is more pronounced in 2000, whereas in 1994, CFC ratios reflect more scatter and a steeper slope. The atmospheric time history of CFC concentration peaked in the early 1990s and began a mild decline before 2000. This change in the source of CFCs to the ocean could account for the greater scatter observed in 1994. Both the 1994 and 2000 data exhibit a strong tendency away from the curvature in the atmospheric input functions. CFC age is calculated by matching the atmospheric time history with the CFC concentration, which yields a ventilation year. The tracer age is the difference between the year of ventilation and the year of sampling.

[32] The frequency distribution of CFC concentration and CFC age shows two distinct peaks separated by a 5–10 year age gap (Figure 10). The differences in midpoint and width of the tracer age distributions for CFC-11, CFC-12 and CFC-113 can be explained by the differences in the atmospheric time history of each CFC [*Sonnerup*, 2001]. Spatially, these peaks correspond to the tracer ages within and below the mixed layer. Given that CFC concentrations are set at the sea surface and subsequently transported into the interior during winter convection, we postulate that the difference in tracer age within and below the mixed layer reflects the residence time of continental shelf water beneath the ice shelf, as well as a dilution effect by the presence of CDW and GMW. For every water parcel in which CFC concentration was measured, we have an estimate of the water mass fraction, which can be used to correct for the dilution bias using the following equation: $CFC = CFC_m/(1 - f_{GMW} - f_{CDW})$, where CFC_m is the measured concentration, f_{GMW} and f_{CDW} are the fractions of GMW and CDW from that water parcel, respectively. The resulting CFC concentration reflects the mean residence time of water in the ice shelf cavity. Both the corrected and uncorrected CFC tracer ages are shown in Figure 11, plotted on top of the transit time age distribution curves generated through the convolution of the atmospheric time history for each CFC with an inverse Gaussian transit time PDF [*Waugh et al.*, 2004]. The inverse Gaussian represents a general parameterization of the combined effects of advection and diffusion, and is also a solution to the 1-D advection diffusion equation [*Hall and Plumb*, 1994; *Waugh et al.*, 2003, 2004]. Each solid line in Figure 11 represents a different ratio of Δ/Γ, where Γ is the mean age and Δ represents the width of the distribution. Γ^2/Δ^2 is equivalent to the Peclet number [*Waugh and Hall*, 2002].

[33] The residence time within the ice shelf cavity is estimated from the difference in mean CFC age within and below the mixed layer. The average tracer ages are listed in Table 3, alongside the mean box model estimates by *Smethie and Jacobs* [2005]. The fit between the TTD curves and the CFC age in the Ross Sea is improved by correcting for the dilution bias of GMW and CDW, but there is still some offset

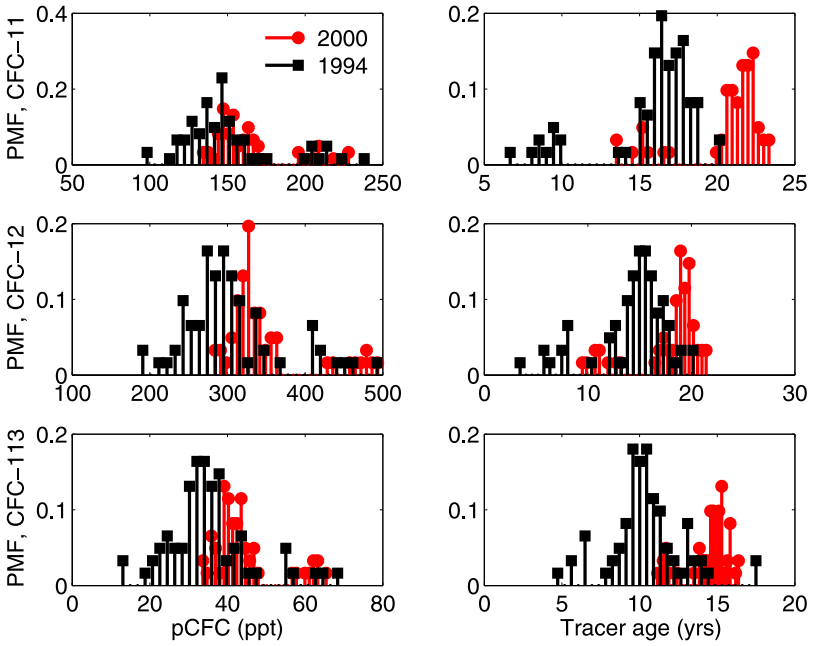

Figure 10. (left) The probability mass function (PMF) of partial gas pressure (pCFC) of CFC-11, 12 and 113 and (right) the PMF of tracer age along the ice shelf front in 1994 and 2000. The difference in concentration and absolute tracer age between 1994 and 2000 reflects the decline of CFCs in the atmosphere from 1994 to 2000.

and scatter between the curves and the data (Figure 11), which may indicate mixing and transport that has not been accounted for by the one-dimensional TTD curves.

4.4. Production and Export of GMW to the Ross Sea

[34] The meltwater flux from underneath the ice shelf is estimated as the product of mean GMW fraction ($\bar{f}$) and the volume of the entire ice shelf cavity, estimated by *Smethie*

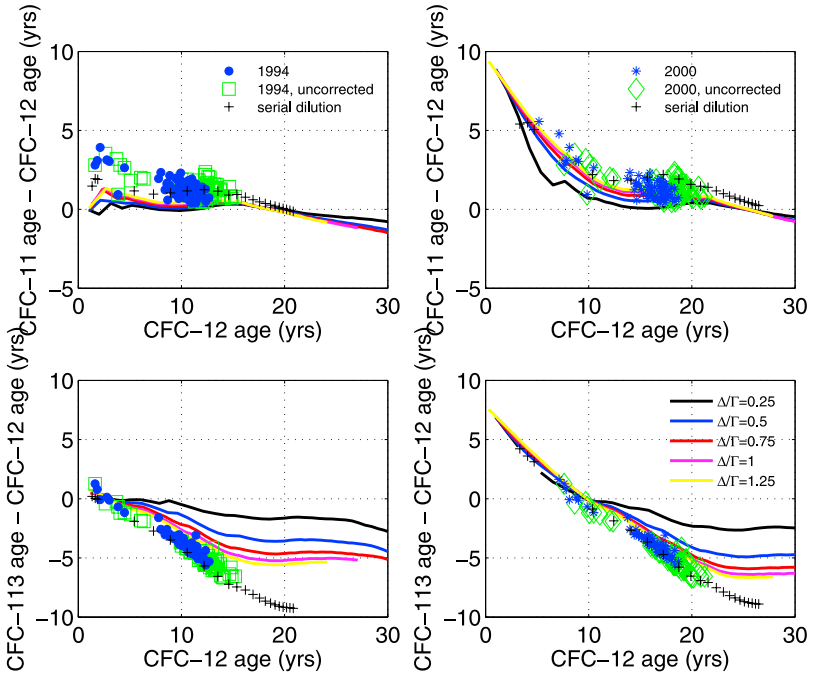

Figure 11. The difference in apparent age between CFC-11 and CFC-12 and CFC-113 and CFC-12, using the atmospheric time history through 1994 and the time history through 2000. The solid lines reflect different ratios of the mean age (Γ) and the width of the age distribution (Δ). The plus symbols represent a hypothetical data set generated by diluting modern CFC concentrations with water containing no detectable CFC concentration. The tracer age relationships from the 2000 and PS94 are plotted separately. The CFC age, corrected for dilution by GMW and CDW, is shown as circles in 1994 and stars in 2000.

Table 3. Estimates of Cavity Residence Time[a]

	Residence Time (GMW Flux)	
	Smethie and Jacobs [2005]	This Study, Average of CFC-11, CFC-12, and CFC-113
1994	4.8 years (33 km^3 a^{-1})	7.5 years (33 km^3 a^{-1})
2000	4.1 years (43 km^3 a^{-1})	5.5 years (50 km^3 a^{-1})

[a]From *Smethie and Jacobs* [2005] and from this study, using differences in CFC age (corrected for dilution by CDW and GMW) within and below the mixed layer. The values presented here, from *Smethie and Jacobs* [2005], are the average of their separate box estimates using CFC-11, CFC-12 and CFC-113.

and Jacobs [2005] (125,300 km^3), divided by the mean residence time. For 1994, $\overline{f}$ = 2.0‰; using a mean residence time of 7.5 years, yields a GMW flux of 33 km^3 a^{-1}. In 2000, the GMW flux was 50 km^3 a^{-1} ($\overline{f}$ = 2.2‰, mean residence time = 5.5 years).

5. Summary and Conclusions

[35] The optimal multiparameter analysis is a simple means to refine the estimates of glacial meltwater concentration derived from conservative tracers. It provides the advantage of easily assessing the sources of uncertainty in the estimate and it minimizes the biases introduced by considering each meltwater tracer individually. For example, we have noted the difficulty in separating the processes that modify the meltwater tracers at the sea surface from the input of basal meltwater at depth. In particular, precipitation and gas exchange affect $\delta^{18}O$ and dissolved oxygen in a manner similar to basal melt, thus creating an artificial meltwater maximum in the mixed layer as seen in 1994. The inclusion of ^4He and Ne in 2000 provided a means to compensate for this bias in the optimal solution. As a visual aid, the OMP method maps water mass fractions to physical space for conceptualization of water mass distributions.

[36] When considering the sources of error in the estimate of water mass concentration, there are three important factors: (1) the effect of uneven sample distribution in the water column, (2) error produced by changes in the water type matrix **C** over time, and (3) bias introduced by using a different suite of tracers to estimate the water mass fraction. Concerning factor 1, the mean GMW concentration is reliable within 5%, on the basis of the bootstrap analysis, and considering factor 2, we estimate that the values in **C** will have changed by less than 5% from 1994 to 2000. In comparison, the variability produced by using different water mass tracers, produced a difference of 23% when both ^4He and Ne were removed. If these three sources of uncertainty are additive, the error in the GMW estimate increases to 33%, or 2.0 ± 0.33‰ in 1994 and 2.2 ± 0.36‰ in 2000. In comparison, *Hohmann et al.* [2002] estimated ~35% uncertainty, including 5% for interpolation errors, in their estimate of GMW for the Amundsen Sea sector, however that study estimated GMW from Ne and ^4He independently and without employing an optimal solution. These results highlight the importance of measuring a consistent suite of water mass tracers to effectively characterize the meltwater concentration at the front of ice shelves. At this stage, we have six well-established meltwater tracers whose coincident measurement produces a superior constraint on the solution. While the estimates from 1994 and 2000 cannot be used to infer a significant trend, a baseline for comparison has been established in 2000 and we anticipate that repeat surveys on a decadal time scale would establish the trend in meltwater concentration.

[37] The distribution of meltwater, at the ice shelf front, indicates regions of high meltwater concentration throughout the eastern section, from the dateline to the east. This feature is most easily observed in the ^4He and Ne concentrations from 2000, but it is also present, if less obvious, in the $\delta^{18}O$ and O_2 from 1994. Lacking samples north of the ice shelf, east of 175°W, it is difficult to determine whether this meltwater is composed entirely of melt from the Ross Ice Shelf or if it reflects another source of meltwater originating outside the Ross Sea.

[38] We have revisited the estimate of residence time underneath the Ross Ice Shelf, employing the same CFC data in 1994 and 2000 used by *Smethie and Jacobs* [2005]. We obtain somewhat different value of mean residence time, within 35 and 47% of their estimate, using a different set of assumptions and a calculation based only on the CFC concentrations. The coincident measurement of the steady state water mass tracers and the transient tracers made it possible to correct the CFC concentrations for mixing and dilution by using the water mass concentrations of CDW and GMW. Our estimates of GMW production; 33 km^3 a^{-1} in 1994 and 55 km^3 a^{-1} are difficult to constrain because of the uncertainty in the residence time estimate, but, coincidentally, the numbers are similar to those of *Smethie and Jacobs* [2005]. Their box model yielded estimates of 29–35 km^3 a^{-1} in 1994 and 36–50 km^3 a^{-1} in 2000. These estimates are not directly comparable as they consider only the outflow of deep Ice Shelf Water whereas our estimate is based on the mean meltwater concentration in the entire cavity, and they mask the differences in residence time. However, our estimate in 2000 is within 5% of the modeled annual average rate of 58 km^3 a^{-1} (13.4 cm a^{-1}) during 2001–2003 [*Dinniman et al.*, 2007]. We use the area of the ice shelf base (4.306×10^5 km^2) to convert from cm to km^3, from the BEDMAP database [*Bamber and Bindschadler*, 1997]. As those authors noted, their melt rate (as well as ours) is on the low end of the range of estimates from a decade ago (12–22 cm a^{-1} or 52–95 km^3 a^{-1}).

[39] This estimate of basal melt rate, like most previous data-based estimates, suffers most from an oversimplification of the circulation dynamics at the ice shelf front. The coherent structure and location of the Ice Shelf Water cores have been repeatedly observed in surveys along the front of the ice shelf (Figure 2). These features indicate flow heterogeneity within the cavity that is not well simplified with cavity-wide approximations. Future estimates may benefit from the assimilation of both transient and steady state tracers into a simple inverse modeling framework to provide a more complete picture of the inflow and outflow at the ice shelf front, and would serve as a comparison to the hydrographic description of flow. *Jenkins and Jacobs* [2008] have attempted this for θ, S and O_2 by assuming of thermal wind balance at the front of the ice shelf. As in this study, the combination of conservative water mass tracers and transient tracers can facilitate a separation between mixing processes, and possibly help distinguish the mean flow from the time-varying component.

[40] **Acknowledgments.** We would like to thank Ralf Weppernig and Roland Hohmann for sample collection and measurement of part of the helium isotope samples, Brent Turrin and Phillippe Collon for measurement of the rest of the helium isotope samples, and Rick Mortlock for measurement of the stable isotope samples. Giancarlo Spezie made it possible for us to collect samples on the Italian research vessel *Italica*. Darryn Waugh provided helpful comments on the transit time distributions. This work was supported by the National Science Foundation through a Fellowship in the IGERT Joint Program (B.L.); by the National Oceanographic and Atmospheric Administration under grants UCSIO PO 10196097-003 (ARCHES) (P.S. and W.M.S.) and ACCWW NA08OAR4320912 (S.J.); by the National Science Foundation under grants OPP 01-25523 and ANT 04-40825 (P.S.); and by the NSF Office of Polar Programs, including 94-18151, 97-25024, and 04-40775 (S.J.). This research was funded in full or in part under the Cooperative Institute for Climate Applications Research (CICAR) from the National Oceanic and Atmospheric Administration, U.S. Department of Commerce. The statements, findings, conclusions, and recommendations are those of the authors and do not necessarily reflect the views of the National Oceanic and Atmospheric Administration or the Department of Commerce. This paper is LDEO contribution 7282.

References

Alley, R. B., P. U. Clark, P. Huybrechts, and I. Joughin (2005), Ice-sheet and sea-level changes, *Science*, *310*, 456–460, doi:10.1126/science.1114613.

Assmann, K., H. H. Hellmer, and A. Beckmann (2003), Seasonal variation in circulation and water mass distribution on the Ross Sea continental shelf, *Antarct. Sci.*, *15*, 3–11, doi:10.1017/S0954102003001007.

Bamber, J. L., and R. A. Bindschadler (1997), An improved elevation dataset for climate and ice-sheet modelling: Validation with satellite imagery, *Ann. Glaciol.*, *25*, 439–444.

Benson, B. B., and D. Krause (1980), Isotopic fractionation of helium during solution: A probe for the liquid state, *J. Solution Chem.*, *9*, 895–909, doi:10.1007/BF00646402.

Bombosch, A., and A. Jenkins (1995), Modeling the formation and deposition of frazil ice beneath Filchner-Ronne Ice Shelf, *J. Geophys. Res.*, *100*, 6983–6992, doi:10.1029/94JC03224.

Budillon, G., M. Pacciaroni, S. Cozzi, P. Rivaro, G. Catalano, C. Ianni, and C. Cantoni (2003), An optimum multiparameter mixing analysis of the shelf waters in the Ross Sea, *Antarct. Sci.*, *15*, 105–118, doi:10.1017/S095410200300110X.

Budillon, G., E. Salusti, and S. Tucci (2006), The evolution of density currents and nepheloid bottom layers in the Ross Sea (Antarctica), *J. Mar. Res.*, *64*, 517–540, doi:10.1357/002224006778715739.

Clarke, W. B., W. J. Jenkins, and Z. Top (1976), Determination of tritium by mass spectrometric measurement of ^{3}H, *Int. J. Radiat. Isotopes*, *27*, 515–522, doi:10.1016/0020-708X(76)90082-X.

Culberson, C. H., and R. T. Williams (1991), A comparison of methods for the determination of dissolved oxygen in seawater, 83 pp., WOCE Hydrogr. Programme Off., Woods Hole, Mass.

Dinniman, M. S., J. M. Klinck, and W. O. J. Smith (2007), Influence of sea ice cover and icebergs on circulation and water mass formation in a numerical circulation model of the Ross Sea, Antarctica, *J. Geophys. Res.*, *112*, C11013, doi:10.1029/2006JC004036.

Epstein, S., and T. Mayeda (1953), Variation of O^{18} content of waters from natural sources, *Geochim. Cosmochim. Acta*, *4*, 213–224, doi:10.1016/0016-7037(53)90051-9.

Fairbanks, R. (1982), The origin of continental shelf and slope water in the New York Bight and the Gulf of Maine: Evidence from $H_2^{18}O/H_2^{16}O$ ratio measurements, *J. Geophys. Res.*, *87*, 5796–5808, doi:10.1029/JC087iC08p05796.

Gordon, A. L., E. Zambianchi, A. Orsi, M. Visbeck, C. F. Giulivi, T. Whitworth III, and G. Spezie (2004), Energetic plumes over the western Ross Sea continental slope, *Geophys. Res. Lett.*, *31*, L21302, doi:10.1029/2004GL020785.

Grootes, P. M., E. J. Steig, and M. Stuiver (1995), The oxygen isotope record from Taylor Dome, Antarctica, *Eos Trans. AGU*, *76*(17), Spring Meet. Suppl., S176.

Hall, T. M., and R. A. Plumb (1994), Age as a diagnostic of stratospheric transport, *J. Geophys. Res.*, *99*, 1059–1070, doi:10.1029/93JD03192.

Hamme, R., and S. Emerson (2004), The solubility of neon, nitrogen and argon in distilled water and seawater, *Deep Sea Res.*, *51*, 1517–1528.

Hohmann, R., P. Schlosser, S. Jacobs, A. Ludin, and R. Weppernig (2002), Excess helium and neon in the southeast Pacific: Tracers for glacial meltwater, *J. Geophys. Res.*, *107*(C11), 3198, doi:10.1029/2000JC000378.

Holland, D., and A. Jenkins (1999), Modeling thermodynamic ice-Ocean interactions at the base of an ice shelf, *J. Phys. Oceanogr.*, *29*, 1787–1800, doi:10.1175/1520-0485(1999)029<1787:MTIOIA>2.0.CO;2.

Holland, D. M., S. S. Jacobs, and A. Jenkins (2003), Modelling the ocean circulation beneath the Ross Ice Shelf, *Antarct. Sci.*, *15*, 13–23, doi:10.1017/S0954102003001019.

Jacobs, S. S., R. G. Fairbanks, and Y. Horibe (1985), Origin and evolution of water masses near the Antarctic Continental Margin: Evidence from $H_2^{18}O/H_2^{16}O$ ratios in seawater, in *Oceanology of the Antarctic Continental Shelf*, *Antarct. Res. Ser.*, vol. 43, edited by S. Jacobs, pp. 59–85, AGU, Washington, D. C.

Jacobs, S. S., H. H. Hellmer, and A. Jenkins (1996), Antarctic ice sheet melting in the southeast Pacific, *Geophys. Res. Lett.*, *23*(9), 957–960, doi:10.1029/96GL00723.

Jacobs, S. S., C. F. Giulivi, and P. A. Mele (2002), Freshening of the Ross Sea during the late 20th century, *Science*, *297*, 386–389, doi:10.1126/science.1069574.

Jenkins, A., and S. Jacobs (2008), Circulation and melting beneath George VI Ice Shelf, Antarctica, *J. Geophys. Res.*, *113*, C04013, doi:10.1029/2007JC004449.

Joughin, I., and L. Padman (2003), Melting and freezing beneath Filchner-Ronne Ice Shelf, Antarctica, *Geophys. Res. Lett.*, *30*(9), 1477, doi:10.1029/2003GL016941.

Lawson, C. L., and R. J. Hanson (1974), *Solving Least Squares Problems*, Prentice Hall, Englewood Cliffs, N. J.

Ludin, A., R. Weppernig, G. Boenisch, and P. Schlosser (1998), Mass spectrometric measurement of helium isotopes and tritium, technical report, Lamont-Doherty Earth Obs., Earth Inst. at Columbia Univ., Palisades, N. Y.

Menke, W. (1989), *Geophysical Data Analysis: Discrete Inverse Theory*, Academic, San Diego.

Mooney, C. Z., and R. D. Duval (1993), *Bootstrapping: A Nonparametric Approach to Statistical Inference*, *Sage Univ. Pap. Ser. Quant. Appl. in the Soc. Sci.*, vol. 07-095Sage, Newbury Park, Calif.

Namiot, A. Y., and E. B. Bukhgalter (1965), Clathrates formed by gases in ice, *J. Struct. Chem.*, *6*, 873–874, doi:10.1007/BF00747111.

Padman, L., S. Erofeeva, and I. Joughin (2003), Tides of the Ross Sea and Ross Ice Shelf cavity, *Antarct. Sci.*, *15*, 31–40, doi:10.1017/S0954102003001032.

Poole, R., and M. Tomczak (1999), Optimum multiparameter analysis of the water mass structure in the Atlantic Ocean thermocline, *Deep Sea Res., Part A*, *46*, 1895–1921, doi:10.1016/S0967-0637(99)00025-4.

Postlethwaite, C. F., E. J. Rohling, W. J. Jenkins, and C. F. Walker (2005), A tracer study of ventilation in the Japan/East Sea, *Deep Sea Res., Part II*, *52*, 1684–1704, doi:10.1016/j.dsr2.2004.07.032.

Press, W. H., S. A. Teukolsky, W. Vetterling, and B. Flannery (1992), *Numerical Recipes in C: The Art of Scientific Computing*, Cambridge Univ. Press, Cambridge, U. K.

Rignot, E., and S. S. Jacobs (2002), Rapid bottom melting near Antarctic ice sheet grounding lines, *Science*, *296*, 2020–2023, doi:10.1126/science.1070942.

Rignot, E., and R. H. Thomas (2002), Mass balance of polar ice sheets, *Science*, *297*, 1502–1506, doi:10.1126/science.1073888.

Rodehacke, C. B., H. H. Hellmer, O. Huhn, and A. Beckmann (2006), Ocean/ice shelf interaction in the southern Weddell Sea: Results of a regional numerical helium/neon simulation, *Ocean Dyn.*, *57*, 1–11, doi:10.1007/s10236-006-0073-2.

Schlosser, P. (1986), Helium: A new tracer in Antarctic oceanography, *Nature*, *321*, 233–235, doi:10.1038/321233a0.

Schlosser, P., R. Bayer, A. Foldvik, T. Gammelsröd, G. Rohardt, and O. K. Münnich (1990), Oxygen 18 and helium as tracers of ice shelf water and water/ice interaction in the Weddell Sea, *J. Geophys. Res.*, *95*, 3253–3263, doi:10.1029/JC095iC03p03253.

Smethie, W. M., and S. S. Jacobs (2005), Circulation and melting under the Ross Ice Shelf: Estimates from evolving CFC, salinity and temperature fields in the Ross Sea, *Deep Sea Res.*, *52*, 959–978, doi:10.1016/j.dsr.2004.11.016.

Sonnerup, R. E. (2001), On the relations among CFC derived water mass ages, *Geophys. Res. Lett.*, *28*, 1739–1742, doi:10.1029/2000GL012569.

Tomczak, M., and D. Large (1989), Optimum multiparameter analysis of mixing in the thermocline of the eastern Indian Ocean, *J. Geophys. Res.*, *94*, 16,141–16,149, doi:10.1029/JC094iC11p16141.

Top, Z., W. Eismont, and W. Clarke (1987), Helium isotope effect and solubility of helium and neon in distilled water and seawater, *Deep Sea Res.*, *34*(7), 1139–1148, doi:10.1016/0198-0149(87)90068-9.

Walker, S. J., R. F. Weiss, and P. K. Salameh (2000), Reconstructed histories of the annual mean atmospheric mole fractions for the halocarbons CFC-11, CFC-12, CFC-113, and carbon tetrachloride, *J. Geophys. Res.*, *105*, 14,285–14,296, doi:10.1029/1999JC900273.

Wanninkhof, R. (1992), Relationship between wind speed and gas exchange over the ocean, *J. Geophys. Res.*, *97*, 7373–7382, doi:10.1029/92JC00188.

Waugh, D. W., and T. M. Hall (2002), Age of stratospheric air: Theory, observations, and models, *Rev. Geophys.*, *40*(4), 1010, doi:10.1029/2000RG000101.

Waugh, D. W., T. M. Hall, and T. W. N. Haine (2003), Relationships among tracer ages, *J. Geophys. Res.*, *108*(C5), 3138, doi:10.1029/2002JC001325.

Waugh, D. W., T. W. N. Haine, and T. M. Hall (2004), Transport times and anthropogenic carbon in the subpolar North Atlantic Ocean, *Deep Sea Res.*, *51*, 1475–1491.

Weppernig, R., P. Schlosser, S. Khatiwala, and R. G. Fairbanks (1996), Isotope data from Ice Station Weddell: Implications for deep water formation in the Weddell Sea, *J. Geophys. Res.*, *101*, 25,723–25,739, doi:10.1029/96JC01895.

Whitworth, T., and A. H. Orsi (2006), Antarctic Bottom Water production and export by tides in the Ross Sea, *Geophys. Res. Lett.*, *33*, L12609, doi:10.1029/2006GL026357.

Zheng, M., W. J. De Bruyn, and E. S. Saltzman (1998), Measurements of the diffusion coefficients of CFC-11 and CFC-12 in pure water and seawater, *J. Geophys. Res.*, *103*(C1), 1375–1379, doi:10.1029/97JC02761. (Correction, *J. Geophys. Res.*, *103*(C10), 21,735, doi:10.1029/98JC02688, 1998.)

S. Jacobs, B. Loose, P. Schlosser, and W. M. Smethie, Lamont-Doherty Earth Observatory, Earth Institute at Columbia University, 61 Route 9W, Palisades, NY 10964, USA. (brice@ldeo.columbia.edu)